



OPEN ACCESS

EDITED BY

Giulio Iovine,
National Research Council (CNR), Italy

REVIEWED BY

Tianbai Zhou,
China Coal Research Institute, China
Marina Muto,
University of Calabria, Italy

*CORRESPONDENCE

Cheng Zhuzhe,
✉ chengcz@minmetals.com

RECEIVED 17 December 2024

ACCEPTED 23 April 2025

PUBLISHED 20 May 2025

CITATION

Zhuzhe C (2025) Analysis of shallow slope instability at an open-pit mine in Fuyang, China.
Front. Earth Sci. 13:1546686.
doi: 10.3389/feart.2025.1546686

COPYRIGHT

© 2025 Zhuzhe. This is an open-access article distributed under the terms of the [Creative Commons Attribution License \(CC BY\)](https://creativecommons.org/licenses/by/4.0/). The use, distribution or reproduction in other forums is permitted, provided the original author(s) and the copyright owner(s) are credited and that the original publication in this journal is cited, in accordance with accepted academic practice. No use, distribution or reproduction is permitted which does not comply with these terms.

Analysis of shallow slope instability at an open-pit mine in Fuyang, China

Cheng Zhuzhe*

Safety and Environmental Protection Department, Minmetals Exploration & Development Co., Ltd., Beijing, China

This study examines the impact of rainfall-induced infiltration on the stability of shallow slopes at the open-pit mine in Fuyang, China. The objective was to elucidate the relationship between rainfall, soil moisture, and landslide initiation. Using COMSOL Multiphysics, the research simulated infiltration effects and identified the strongly weathered limestone at +250 m as a critical stability factor. Results showed increased pore water pressure and saturation levels with rainfall, particularly affecting the unsaturated zone. A high-risk landslide area was pinpointed between +250 m and +270 m. To mitigate risks, a reinforcement strategy with mini steel pipe piles was proposed. The study underscores the need for integrated data in predictive models to enhance landslide risk management in mining and other landslide-prone regions.

KEYWORDS

shallow slope, rainfall infiltration, multi-physics model, numerical simulation, safety

1 Introduction

In hilly and mountainous terrains (Anagnostopoulos et al., 2015; Nadim et al., 2006; Yuan et al., 2021), shallow landslides pose formidable threats to communities, infrastructure, and the environment, constituting a critical focus in geohazard research. These events exhibit strong rainfall dependency, with extreme precipitation amplifying landslide susceptibility through rapid soil moisture variation, pore-water pressure escalation, and slope destabilization (Borgomeo et al., 2014). While statistical models (Pantelidis, 2009; Lü et al., 2024; Rosi et al., 2012) demonstrate efficacy in regional landslide susceptibility mapping, their capacity to elucidate physical failure mechanisms remains limited. This knowledge gap (Ali et al., 2014; Caleca et al., 2022; Moore et al., 1991) stems from the complex interplay of subsurface hydrological processes regulated by soil properties (Ng, 2006), topographic features (Ohlmacher, 2007), and antecedent moisture conditions (Zhang et al., 2024). Particularly, the rainfall-initiation mechanisms of shallow landslides retain unresolved complexities, as current models inadequately capture the spatiotemporal evolution of slope hydromechanical responses (Sidle and Bogaard, 2016; Wang et al., 2019; Löbmann et al., 2020; Matsushi et al., 2006).

Recent advancements integrate multi-physics modeling with copula dependence structures to enhance slope reliability analysis under coupled slope cutting and rainfall conditions, providing probabilistic tools for copula selection and slope management

decision-making (Liu et al., 2024). Experimental validation (Feng et al., 2024) through shaking table tests by Feng et al. revealed tension-shear failure mechanisms in bedrock slopes under seismic-rainfall coupling, demonstrating the critical role of foot anti-sliding forces and soil-bedrock interface characteristics in slope stability. Building upon these findings, Wang et al. (2024) developed an optimized monitoring framework employing finite element-based orthogonal testing to improve rainfall infiltration simulation accuracy, particularly applied to slope hydrological response analysis in Sichuan Province. Further methodological refinement (Wang et al., 2023) was achieved through deterministic limit equilibrium analysis for critical failure surface identification, with validated predictive capability for rainfall-induced landslide scenarios.

This study presents a holistic investigation into the impact of rainfall on the initiation of shallow landslides. The multi-physics model is introduced that delves into the intricate interactions between surface and subsurface hydrology and the onset of shallow landslides. The model incorporates a variably saturated flow framework, accounts for rainfall infiltration phenomena in shallow slope. The geotechnical component of the model is anchored in a multi-physics analysis, which adheres to the foundational principles of unsaturated soil mechanics (Bordoloi et al., 2020).

The study culminates by underscoring the imperative of integrating hydrological, geological, and topographical data into predictive models. Such integration is vital for enhancing our capacity to anticipate landslide risks and execute effective mitigation strategies. Grasping the intricate interplay between these factors is especially crucial in developing regions that are prone to landslides and are experiencing increasing population growth and development pressures.

2 Materials and methods

2.1 Description of the Fuyang open-pit mine

The open-pit mine, located in Fuyang, Zhejiang Province, China, experienced a landslide on its eastern slope in March 2015. This geological event was triggered by the infiltration of continuous heavy rainfall, leading to the failure of a silty clay layer, measuring 22 to 34 m in thickness at the slope's crest. The resulting landslide displaced approximately 6,000 cubic meters of soil, qualifying it as a small-scale soil landslide. Following the incident, the affected area has been successfully stabilized and re-vegetated with the planting of Moso bamboo. Drainage ditches, extending 350 m in length, have been meticulously installed along the crest of the rehabilitated slope within the treatment zone. These measures have proven effective, as no subsequent landslides have been reported in this particular section since their installation. The present state of the mining area's slopes is illustrated in Figure 1, which the zone within the scope of the red dash line is the historical landslide area.

Despite these remedial measures, the lower sections of the mining area still necessitate further extraction. Consequently, the stability of the shallow soil slopes within the mining area is crucial for the safe and continued mining operations in the lower regions.

The open-pit mining operation employs a top-down, bench-by-bench mining approach, characterized by horizontal advancement, deep-hole blasting, excavator loading, and transportation via dump trucks. Mechanical stripping is utilized for the removal of overburden. Each bench stands at a height of 15 m with a working slope angle of 75°. Field measurements indicate that the maximum height of the resulting slope exceeds 200 m. Given the primary focus on the stability of the upper section, which consists of weathering rock and silty clay, under the impact of rainfall, a detailed stability analysis of this specific region (as depicted in Figure 2) is conducted under simulated rainfall conditions. The context of this study revolves around the potential for slope failure and landslides.

2.2 Shallow slope and its parameters

Relying on field survey data, the maximum height of the slope that was ultimately shaped surpasses 200 m, coinciding with a zone where a previous collapse had occurred. The study's emphasis is on evaluating the stability of the upper section of the slope, which is composed of silty clay interspersed with fragmented stones, particularly under the impact of rainfall. A targeted stability analysis under rainy conditions is executed specifically for this section, as illustrated in Figure 2.

The geological survey report from the open-pit mine outlines the key mechanical parameters of the rock formations in Table 1. These parameters were ascertained through a suite of laboratory tests, as shown in Figure 3, and through water injection and pumping tests to assess permeability and other fluid-related characteristics. The cylindrical rock sample illustrated in Figure 3 has standard dimensions of 10 cm in height and 5 cm in diameter. Triplicate rock specimens were prepared for each experimental condition.

For the medium weathering limestone, the determination of its parameters was achieved via uniaxial compression testing, with subsequent refinements in line with the Hoek-Brown criterion to account for weathering effects and other environmental influences.

The acquisition of undisturbed samples from the silty clay and the strongly weathering granite presented significant challenges, thus precluding conventional laboratory mechanical testing. Consequently, the survey team had to rely on a synthesis of existing literature, established geological standards, and local engineering experience to establish the physical and mechanical parameters for these two rock strata. The study adopts these parameters, after careful consideration, deeming them to be rational and suitable for the computational analyses undertaken.

2.3 Methodology for assessing slope instability induced by rainfall infiltration

In this study, COMSOL Multiphysics is utilized to simulate and assess the influence of rainfall infiltration on the stability of slopes. The Richards equation is used, which posits that fluids flow through porous media like soil, with water being able to move freely within the pore spaces. This equation is versatile under both unsaturated and saturated conditions, adept at capturing the infiltration process of water from the soil surface to deeper strata and the subsequent vertical movement of moisture within



FIGURE 1
Open-pit mine area.

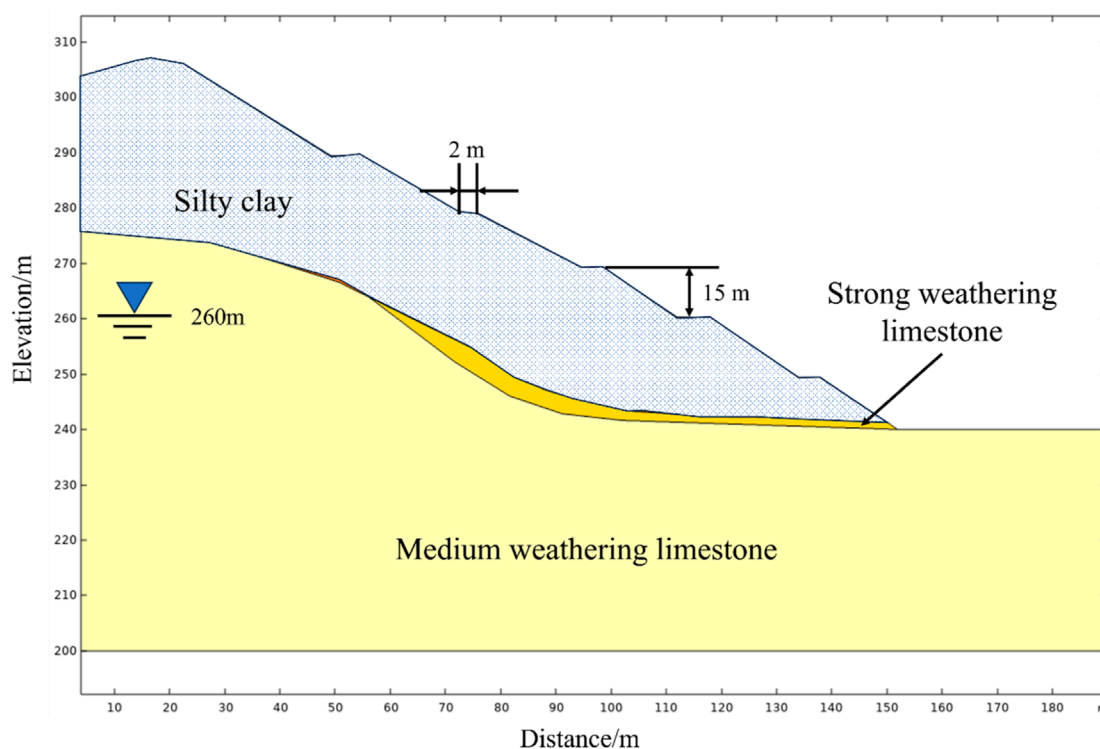


FIGURE 2
Rock type and size of the shallow slope model.

the soil. It assumes that the fluid is incompressible and flows at a constant temperature, disregarding the impact of temperature fluctuations on the fluid's properties. Given that the scope of our research centers on the upper portion of the slope, which is predominantly composed of crushed stone silty clay and strongly weathering limestone, the Richards equation is particularly apt for studying the effects of rainfall infiltration on slope stability within

saturated-unsaturated flow conditions. For the saturated seepage within geotechnical materials, where pore water pressure is the key variable, Darcy's law is relied on to articulate the behavior of fluid flow (Equation 1).

$$u = -\frac{K_s}{\rho g}(\nabla p + \rho g \nabla D) \tag{1}$$

TABLE 1 Mechanical parameters of slope rock mass.

Parameters	Silty clay	Strongly weathering limestone	Medium weathering limestone
Cohesion strength/c(kPa)	20	200	320
Internal friction angle/ $\varphi(^{\circ})$	22.5	27.0	33.5
Elastic modulus/E(GPa)	1.5	3.0	3.7
Poisson ratio/ μ	0.28	0.22	0.25
Unit weight/ $\gamma(\text{kN}/\text{m}^3)$	1.5	3.0	3.7
Permeability coefficient(m/d)	18.8	22.5	26.9



FIGURE 3 Medium weathering limestone sample of experimental test.

where the u is the flow velocity (m/s), K_s is the saturated permeability coefficient (m/s), ρ is the density of water (kg/m^3), g is the gravity (N/kg), p is pore pressure (Pa), D is the elevation (m).

In the case of unsaturated flow, with the air within the soil and rock being subject to atmospheric pressure, the Richards equation (Gengqian et al., 2020) is employed to characterize the phenomenon in Equations 2–5.

$$[C + SeS] \frac{\partial H_p}{\partial t} + \nabla \cdot [-K \nabla (H_p + D)] = 0 \quad (2)$$

TABLE 2 Hydraulic parameters of numerical simulation in shallow slope model.

Parameters	Value
Saturated Volumetric Water Content θ_s	0.5
Residual Volumetric Water Content θ_r	0.06
α	1
n	1.5
l	0.5
Thickness of Infiltration Boundary/L(m)	0.01
Depth of Standing Water/ H_w (m)	0.5

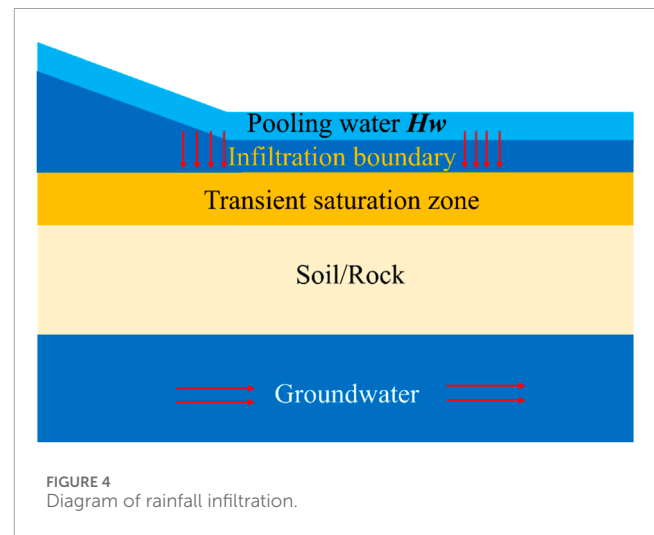


FIGURE 4 Diagram of rainfall infiltration.

$$C = \frac{\partial \theta}{\partial H_p} \quad (3)$$

$$S = \rho g (\delta_p + \theta \delta_f) \quad (4)$$

$$K = K_s k_r \quad (5)$$

where C denotes the specific moisture capacity (m^{-1}), S_e is the effective saturation, S is the storage coefficient (m^{-1}), t represents time, K is the unsaturated permeability coefficient (m/s), θ is the volumetric water content, δ_p and δ_f are the compressibilities of the solid and fluid phases ($\text{m} \cdot \text{s}^2/\text{kg}$), and k_r is the relative permeability. The primary challenge in describing the movement of fluids in variable-saturated porous media lies in characterizing the changes in the transmission and storage capacities of fluids as they enter and fill the pore spaces. However, data for these properties are often difficult to obtain through experiments. The unsaturated hydraulic parameters C , S_e , θ and k_r are calculated using the built-in Van Genuchten model in COMSOL Multiphysics. By combining the saturated and unsaturated seepage equations, the rainfall infiltration is derived by Equation 6.

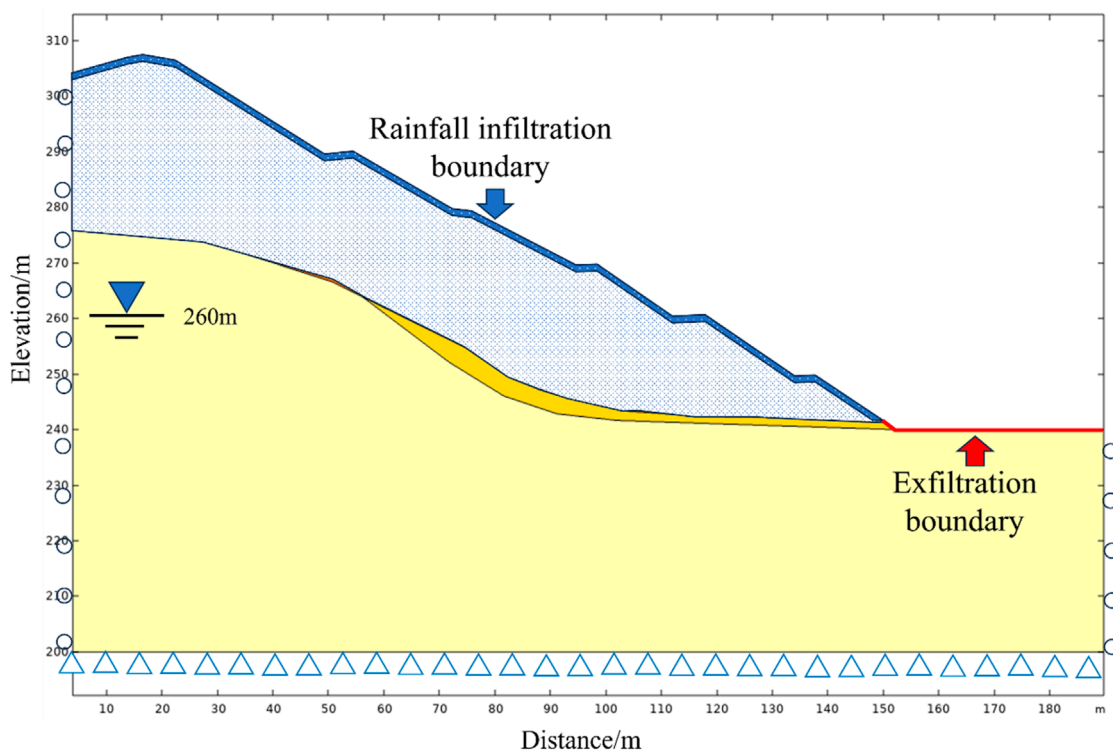


FIGURE 5 Boundary condition of rainfall infiltration.

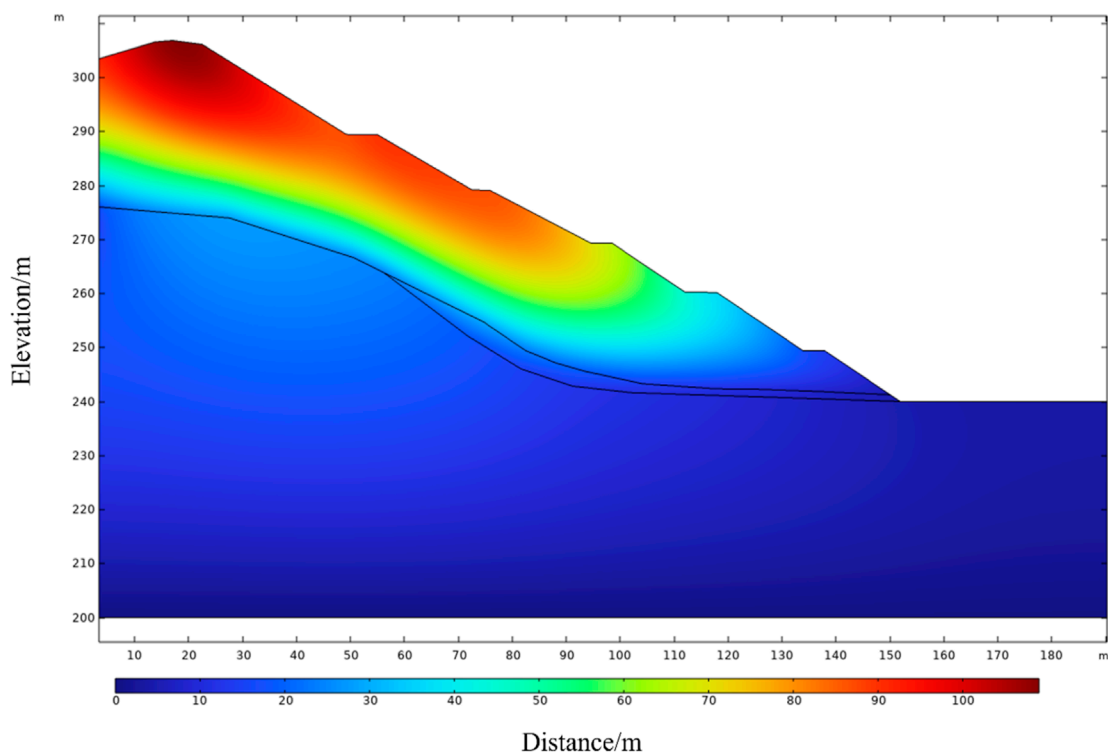
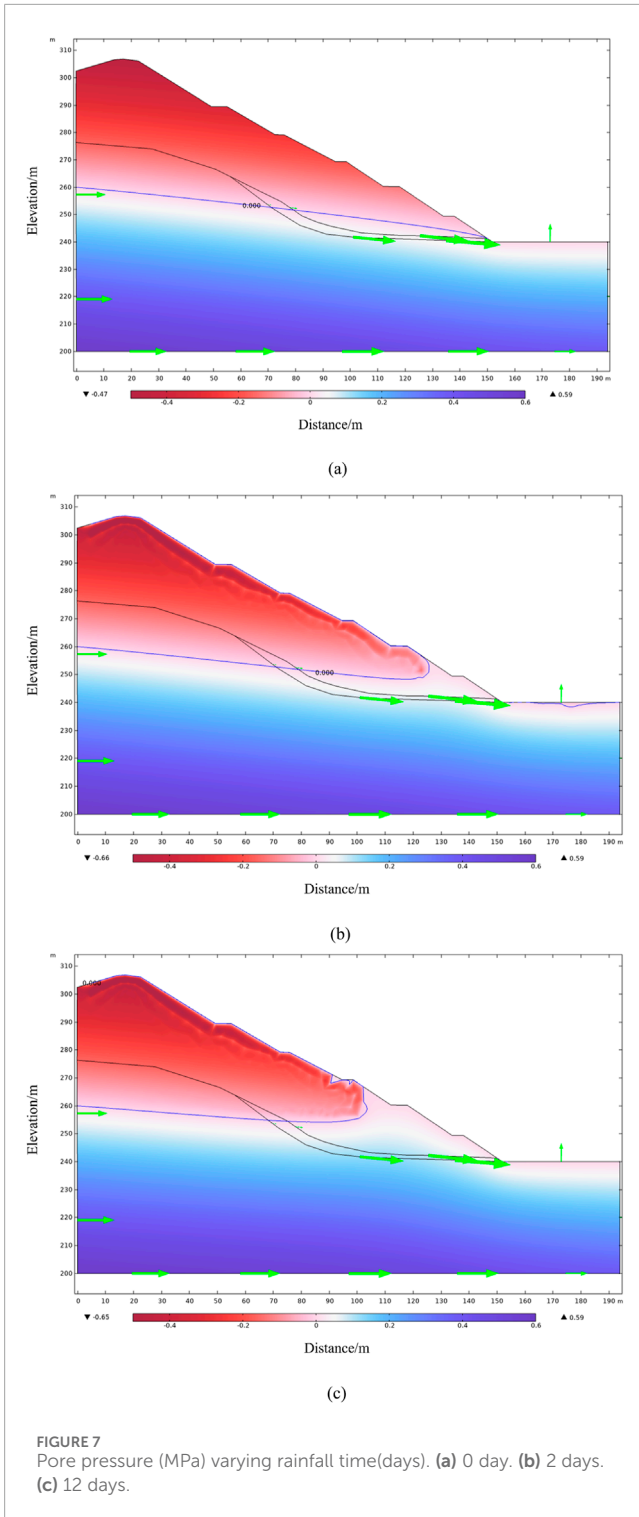


FIGURE 6 Initial displacement of slope under the gravity.



$$-n \cdot \rho u = \rho \frac{K_s}{L} \left(H_w - \frac{p}{\rho g} \right) \quad (6)$$

where the n is normal vector of the boundary, L is the thickness of the infiltration boundary condition (m), and H_w represents the water depth (m). The values of L and H_w cannot be accurately obtained and are both based on empirical values. Figure 3 shows a schematic diagram of the slope with water infiltration, and the hydraulic parameters related to numerical simulation are shown in Table 2.

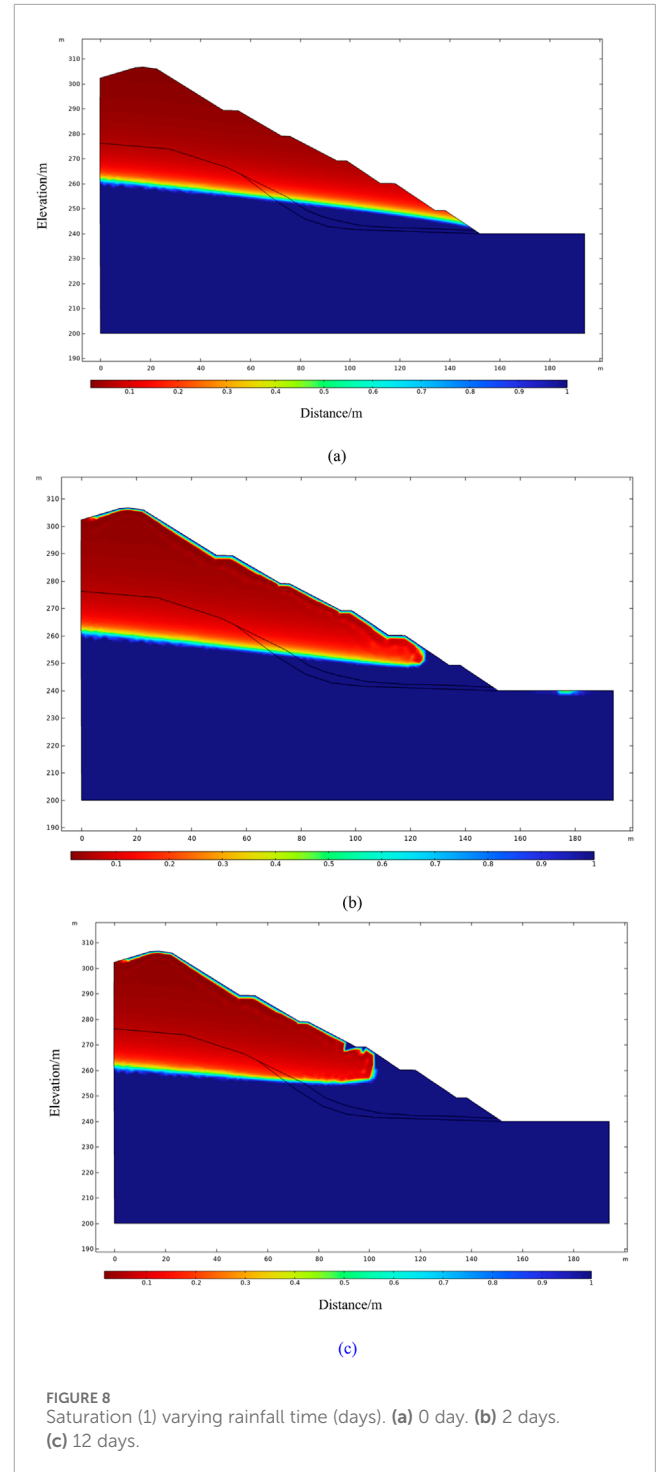
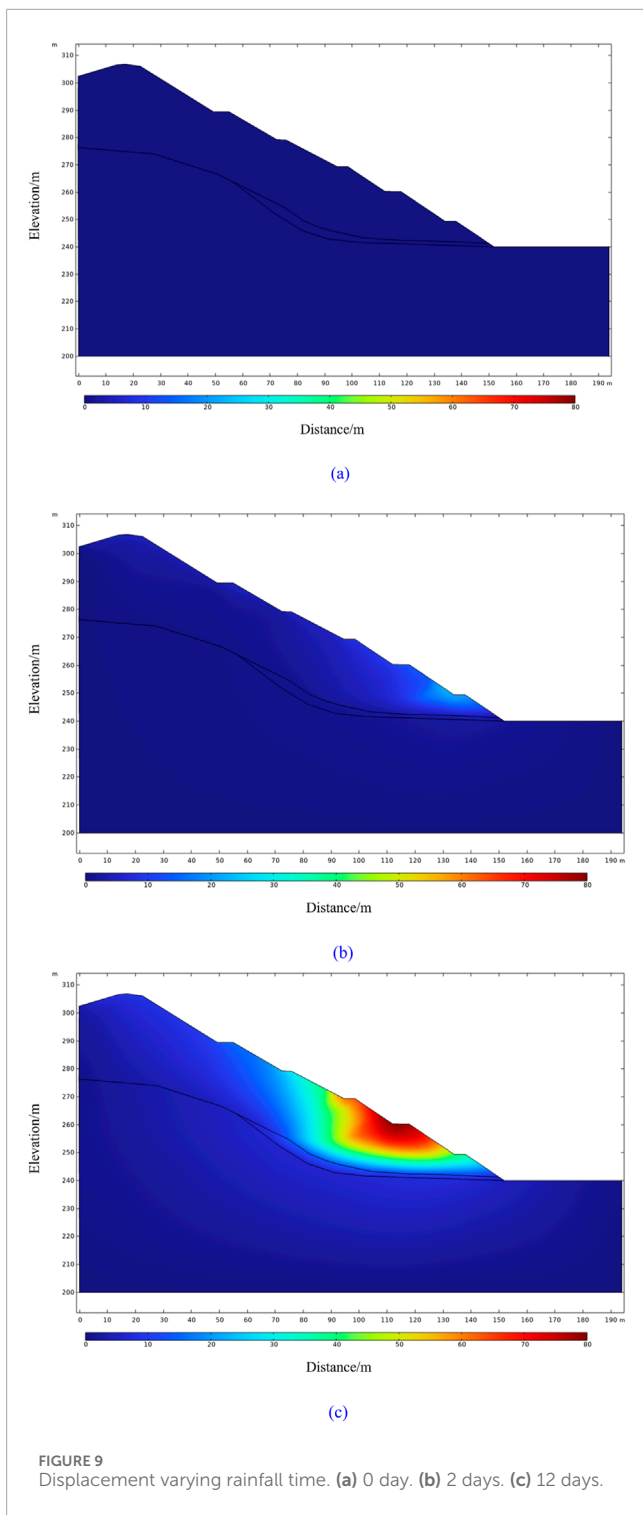


Figure 4 encapsulates the intricate process of rainfall-induced infiltration on a slope, a critical mechanism in the context of shallow landslides. At the onset of rainfall, water pools on the surface (H_w), potentially increasing pore-water pressure and destabilizing the slope. This pooled water signifies the initial stressor on the slope. As the soil reaches its infiltration capacity, the pooling water transitions into the subsurface, marking the infiltration boundary—a critical juncture where subsurface flow commences to impact slope stability. Below this boundary, the transient saturation zone forms, where



soil or rock saturation occurs, temporarily reducing soil resistance to shear and heightening the risk of slope failure. The soil/rock's permeability is a key factor in this sequence, influencing the rate of water infiltration and the subsequent formation of the transient saturation zone. This, in turn, affects the groundwater table, which can rise in response to intense or prolonged rainfall, further exacerbating the pressure on the slope and increasing the likelihood of a landslide.

2.4 Principles and basic assumptions of slope stability analysis

In COMSOL, slope stability is assessed by parameterizing material properties and the factor of safety (FOS). The study incrementally raises the FOS while decrementally adjusting the mechanical parameters of the soil and rock. A non-converging model indicates potential slope failure. This numerical simulation incorporates the Mohr-Coulomb yield criterion (Zeng et al., 2018) in Equations 7–9, factoring in the influences of pore pressure and gravity.

$$F = \sqrt{J_2} + \frac{\sin \varphi}{3} I_1 - C \cos \varphi \quad (7)$$

$$C_f = \frac{c_f}{FOS} \quad (8)$$

$$\varphi = \text{atan}\left(\frac{\tan \varphi_u}{FOS}\right) (p < 0) + \text{atan}\left(\frac{\tan \varphi_s}{FOS}\right) (p > 0) \quad (9)$$

where C_f is the cohesion stress related with the c_f and FOS, φ_u and φ_s represent the internal friction angles for unsaturated and saturated soil/rock respectively, and p represents the pore water pressure generated during saturated-unsaturated seepage flow.

Given the intricate geological conditions of the mine in Figure 5, the numerical simulation and computation processes are predicated on the following fundamental assumptions:

- 1) The geological formations are presumed to be isotropic, implying uniform material properties in all directions, and locally homogeneous, suggesting a consistent distribution of these properties within localized regions.
- 2) The model is designed with fixed supports at the base and roller supports on the sides, permitting vertical displacement only. The slope surface is defined by rainfall infiltration boundary conditions. It is posited that the lowest tier of the existing slope serves as a seepage outlet. The total water head on the left is estimated to be around 260 m, based on engineering geological findings, while the water head on the right is set at 240 m.
- 3) The influence of geological features, including fractures and fissures within the soil and rock mass, has been integrated by adjusting the mechanical parameters in accordance with outcomes from experimental data and recommendations derived from the engineering survey.
- 4) The rainfall intensity for the open-pit mining area is determined by the Department of Housing and Urban-Rural Development of Zhejiang Province. The calculated maximum daily rainfall is 254.2 mm/day, which is utilized as the boundary condition for rainfall infiltration in the model.

3 Results

3.1 Analysis in solver

Displacement is pivotal in assessing the stability of slopes, with excessive movement potentially triggering landslides and platform collapses. The analysis of displacement is particularly concentrated at the slope's toe. To address this, the COMSOL software is utilized to simulate the process of rainfall infiltration across three steps.

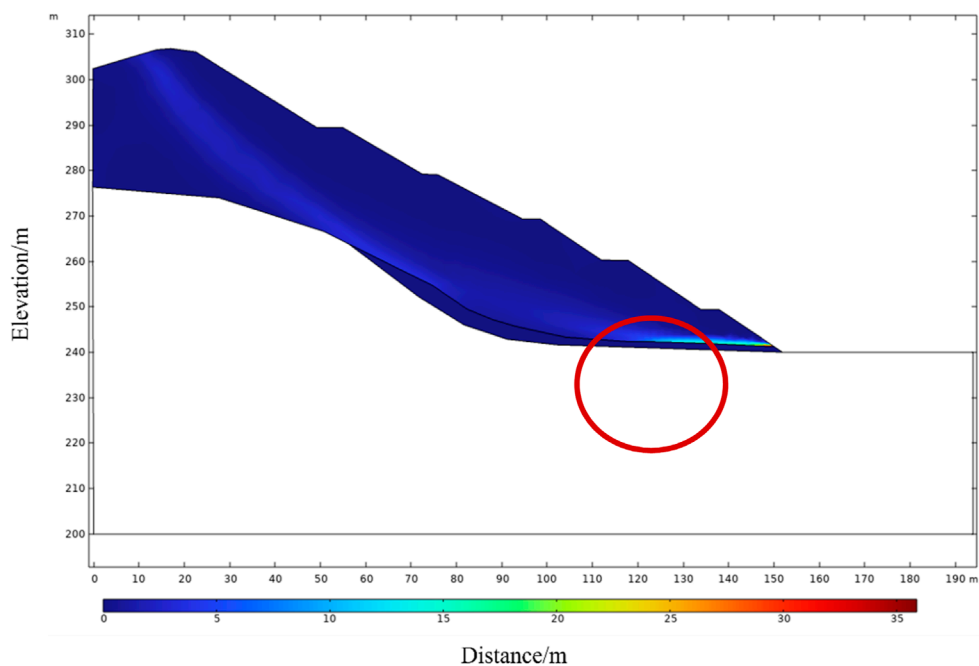


FIGURE 10
Plastic strain after 12 days.

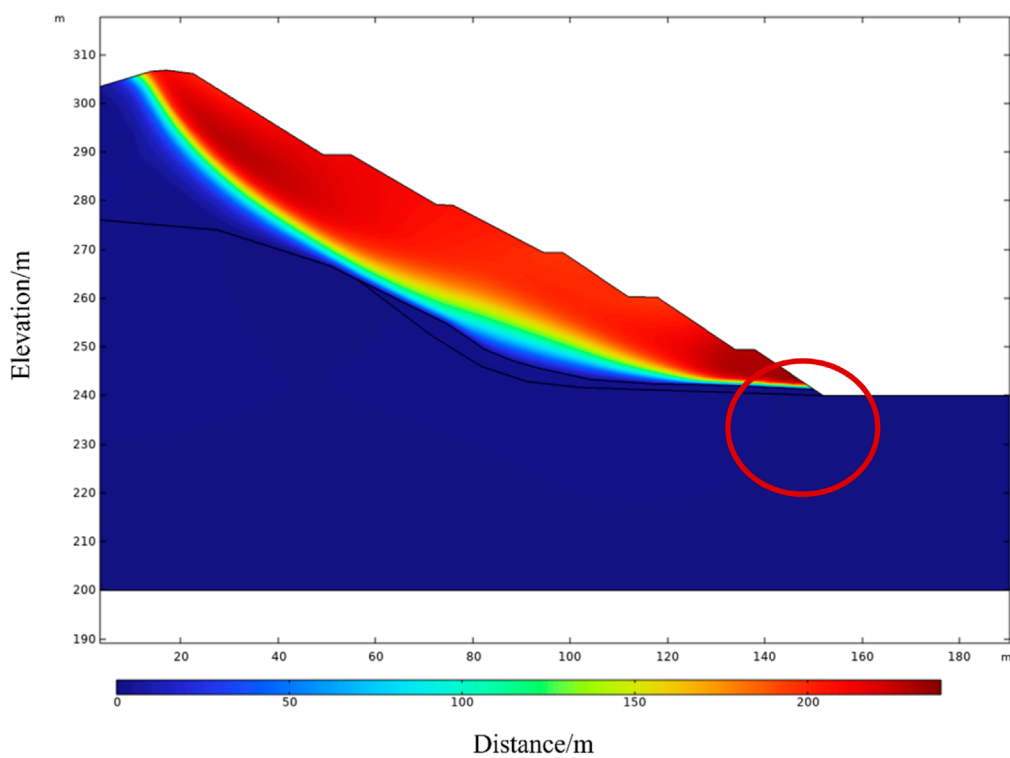


FIGURE 11
Displacement of shallow slope at critical landslide state (FOS = 1.25).



FIGURE 12
Slope reinforcement with mini steel pipe piles.

- 1) The simulation of the original stress conditions at the commencement of the rainfall period, day 0, is initiated, focusing on steady-state saturated seepage and stress conditions.
- 2) Based on the first step, the dynamic changes in seepage and stress within the slope over a 12-day rainfall scenario are modeled, examining the transient behavior of saturated-unsaturated seepage and stress conditions.
- 3) Finally, leveraging the insights from the second phase, the pattern of displacement across the benches of an open-pit mine under varied rainfall conditions is simulated, employing a strength reduction approach to predict the behavior of the slope under these conditions.

The displacement cloud map of the original open-pit mine is shown in Figure 6, where the displacement at the top of the slope under the influence of gravity is about 100 mm, which has a significant impact on the study of the stress-strain state of the slope under rainfall conditions. Therefore, when conducting the calculations for Study 2, by using the “Pre-stress and Pre-strain” node in COMSOL software, the stress-strain state solved in Study one can be inherited to eliminate the influence of the original rock stress.

3.2 Pore pressure in slope with time under rainfall

As shown in Figure 7, the distribution of pore water pressure in the slope corresponding to different rainfall durations is displayed, where the blue solid line represents a pore pressure of 0 MPa. Below this line, as the height decreases, the pore water pressure gradually increases, with a maximum value of 0.59 MPa. In the shallow slope near the slope face, the pore water pressure is less than 0, indicating

the absence of pore water pressure, and the value has no specific physical meaning. The green arrows represent the direction of water flow. Figure 7A shows the distribution of pore water pressure at day 0, with water seeping out from the toe of the slope. After 2 days of rainfall in Figure 7B, the area of the blue solid line becomes smaller, indicating that rainfall has increased the pore water pressure in the shallow slope, leading to changes in the distribution of the unsaturated zone, with the area below +250 m becoming saturated. After 12 days of rainfall in Figure 7C, the unsaturated zone further shrinks, and the area below +240 m becomes a saturated zone.

3.3 Saturation in slope with time under rainfall

As shown in Figure 8, the distribution of saturation in the shallow slope under varying rainfall durations is depicted. Saturation ranges from 0 to 1, with 0 indicating complete unsaturation and one indicating complete saturation, and intermediate values representing varying degrees of unsaturation. At the initial state (0 days), the saturated areas correspond exactly to the pore pressure distribution shown in Figure 7A, where regions with pore pressure greater than 0 are all saturated areas. As the duration of rainfall increases in Figure 8B, the saturation of the shallow slope surface undergoes changes. By the rainfall duration time reaches 12 days, the unsaturated areas are significantly reduced, and all areas below +260 m have become saturated regions.

3.4 Identification of critical failure surfaces and potential failure zones

Figure 9 illustrates the distribution of displacement in the shallow slope under varying rainfall durations. At the initial state (Figure 9A), the slope exhibits no displacement, as the effects of gravity have been mitigated. After 2 days of rainfall (Figure 9B), a minor displacement of approximately 20 mm is observed at the +250 m elevation. Upon reaching 12 days of rainfall (Figure 9C), a significant displacement of about 80 mm occurs between the +250 m and +270 m levels, suggesting that this area may be at risk of a landslide.

4 Discussion

Figure 10 displays the plastic strain in the shallow slope, with the maximum plastic strain value of around 20% occurring within the strongly weathering limestone between +240 m and +250 m. It is believed that the cause of the landslide in this area is rainfall, which has transformed the unsaturated zone below +250 m into a saturated zone, leading to a reduction in rock mechanical parameters and causing significant strain in the strongly weathering limestone, which in turn affects the displacement of the upper soil and rock slope.

Figure 11 illustrates the critical state of the shallow slope after 12 days of rainfall, at which the Factor of Safety (FOS) is 1.25. It can be observed from the figure that the maximum displacement

at the +250 m bench exceeds 200 mm, and the overall slope exhibits a circular arc sliding pattern.

Based on these simulation results, it is believed that the key area affecting the overall stability of the shallow slope is the strongly weathered limestone at +250 m, and therefore reinforcement treatment is needed for this area (Figure 12). A total of 54 mini steel pipe piles are arranged in two rows, with a pile spacing of 2.5 m and a row spacing of 2.5 m. The length of each pile is 30 m, with the lower 15 m being equipped with 80 mm diameter steel pipes. For the rear row of piles (on the mountain side), the anchorage length below the potential slip surface is approximately 10 m, and the length of the steel pipe above the slip surface is about 5 m, with a drilling burial depth (backfill depth) of 15 m. For the front row of piles, the anchorage length below the potential slip surface is about 8 m, and the length of the steel pipe above the slip surface is about 7 m, with a drilling burial depth of 15 m.

5 Conclusion

This study employed numerical simulation to establish a dynamic evolution model of slope stability under rainfall infiltration. Numerical simulations revealed that prolonged rainfall duration significantly increases pore water pressure and saturation levels within the slope, while markedly altering the spatial distribution characteristics of unsaturated zones. Notably, the rainfall infiltration process accelerates phase transformation from unsaturated to saturated zones, triggering deterioration of rock mechanical parameters and substantial strain accumulation in limestone layers, ultimately resulting in significant displacement responses in both overburden soil and bedrock slopes. Displacement field analysis demonstrated maximum deformation magnitudes within the +250 m to +270 m elevation range, with vector distribution patterns indicating high landslide susceptibility in this critical zone. To address stability concerns, the research team proposed a composite reinforcement system consisting of 54 micro steel pipe piles arranged in a double-row quincuncial configuration, which effectively enhances slope integrity through optimized soil-pile interaction mechanisms. The developed rainfall-induced slope failure model, incorporating field monitoring data and fluid-solid coupling constitutive equations, innovatively achieves quantitative early warning of slope instability, providing robust theoretical foundations and technical references for geological hazard prevention in similar engineering projects.

References

- Ali, A., Huang, J., Lyamin, A., Sloan, S., Griffiths, D., Cassidy, M., et al. (2014). Simplified quantitative risk assessment of rainfall-induced landslides modelled by infinite slopes. *Eng. Geol.* 179, 102–116. doi:10.1016/j.enggeo.2014.06.024
- Anagnostopoulos, G., Fatichi, S., and Burlando, P. (2015). An advanced process-based distributed model for the investigation of rainfall-induced landslides: the effect of process representation and boundary conditions. *Water Resour. Res.* 51, 7501–7523. doi:10.1002/2015wr016909
- Bordoloi, S., Ni, J., and Ng, C. W. W. (2020). Soil desiccation cracking and its characterization in vegetated soil: a perspective review. *Sci. Total Environ.* 729, 138760. doi:10.1016/j.scitotenv.2020.138760
- Borgomeo, E., Hebditch, K. V., Whittaker, A. C., and Lonergan, L. (2014). Characterising the spatial distribution, frequency and geomorphic controls on landslide occurrence, Molise, Italy. *Geomorphology* 226, 148–161. doi:10.1016/j.geomorph.2014.08.004
- Caleca, F., Tofani, V., Segoni, S., Raspini, F., Franceschini, R., and Rosi, A. (2022). How can landslide risk maps be validated? Potential solutions with open-source databases. *Front. Earth Sci.* 10. doi:10.3389/feart.2022.998885
- Feng, H., Jiang, G., He, Z., Guo, Y., He, X., He, B., et al. (2024). Dynamic response and failure characteristics of a slope with bedrock subjected to earthquakes and rainfall in shaking table tests. *Bull. Eng. Geol. Environ.* 83 (7), 265. doi:10.1007/s10064-024-03748-0
- Gengqian, N., Zhonghui, C., Lingfan, Z., Ming, B., and Zihan, Z. (2020). Treatment of two boundary conditions for rainfall infiltration in slope and its application. *Rock Soil Mech.* 41 (12), 4105–4115. doi:10.16285/j.rsm.2020.0338 (in Chinese).

Data availability statement

The original contributions presented in the study are included in the article/supplementary material, further inquiries can be directed to the corresponding author.

Author contributions

CZ: Conceptualization, Data curation, Formal Analysis, Funding acquisition, Investigation, Methodology, Project administration, Resources, Software, Supervision, Validation, Visualization, Writing – original draft, Writing – review and editing.

Funding

The author(s) declare that financial support was received for the research and/or publication of this article. This work was supported by the Heilongjiang Provincial Major Scientific and Technological Achievements Transformation Project (grant number CG23025).

Conflict of interest

Author CZ was employed by Minmetals Exploration & Development Co., Ltd.

Generative AI statement

The authors declare that no Generative AI was used in the creation of this manuscript.

Publisher's note

All claims expressed in this article are solely those of the authors and do not necessarily represent those of their affiliated organizations, or those of the publisher, the editors and the reviewers. Any product that may be evaluated in this article, or claim that may be made by its manufacturer, is not guaranteed or endorsed by the publisher.

- Liu, L.-L., Xu, Y. B., Zhu, W. Q., Zallah, K., Huang, L., and Wang, C. (2024). Reliability analysis of cutting slopes under rainfall conditions considering copula dependence between shear strengths. *Stochastic Environmental Research and Risk Assessment* 38 (10), 3985–4006. doi:10.1007/s00477-024-02789-x
- Löbmann, M., Geitner, C., Wellstein, C., and Zerbe, S. (2020). The influence of herbaceous vegetation on slope stability – a review. *Earth-Science Reviews* 209, 103328. doi:10.1016/j.earscirev.2020.103328
- Lü, Q., Wu, J., Liu, Z., Liao, Z., and Deng, Z. (2024). The Fuyang shallow landslides triggered by an extreme rainstorm on 22 July 2023 in Zhejiang, China. *Landslides* 21, 2725–2740. doi:10.1007/s10346-024-02314-9
- Matsushi, Y., Hattajji, T., and Matsukura, Y. (2006). Mechanisms of shallow landslides on soil-mantled hillslopes with permeable and impermeable bedrocks in the Boso Peninsula, Japan. *Geomorphology* 76, 92–108. doi:10.1016/j.geomorph.2005.10.003
- Moore, I., Grayson, R., and Ladson, T. (1991). Digital terrain modelling: a review of hydrological, geomorphological, and biological applications. *Hydrological Processes* 5, 3–30. doi:10.1002/hyp.3360050103
- Nadim, F., Kjekstad, O., Peduzzi, P., Herold, C., and Jaedicke, C. (2006). Global landslide and avalanche hotspots. *Landslides* 3, 159–173. doi:10.1007/s10346-006-0036-1
- Ng, K. Y. (2006). Landslide locations and drainage network development: a case study of Hong Kong. *Geomorphology* 76, 229–239. doi:10.1016/j.geomorph.2005.10.008
- Ohlmacher, G. (2007). Plan curvature and landslide probability in regions dominated by earth flows and earth slides. *Engineering Geology* 91, 117–134. doi:10.1016/j.enggeo.2007.01.005
- Pantelidis, L. (2009). Rock slope stability assessment through rock mass classification systems. *International Journal of Rock Mechanics and Mining Sciences* 46 (46), 315–325. doi:10.1016/j.ijrmms.2008.06.003
- Rosi, A., Segoni, S., Catani, F., and Casagli, N. (2012). Statistical and environmental analyses for the definition of a regional rainfall threshold system for landslide triggering in Tuscany (Italy). *Journal of Geographical Sciences* 22, 617–629. doi:10.1007/s11442-012-0951-0
- Sidle, R., and Bogaard, T. (2016). Dynamic earth system and ecological controls of rainfall-initiated landslides. *Earth-Science Reviews* 159, 275–291. doi:10.1016/j.earscirev.2016.05.013
- Wang, C. H., Fang, L., Chang, D. T. T., and Huang, F. C. (2023). Back-analysis of a rainfall-induced landslide case history using deterministic and random limit equilibrium methods. *Engineering Geology* 317, 107055. doi:10.1016/j.enggeo.2023.107055
- Wang, F., Chen, F., Deng, H., Zhao, J., Chen, J., Xu, W., et al. (2024). An improved monitoring strategy for shallow rainfall-induced landslides under critical site-specific recognition. *Landslides* 21, 2569–2581. doi:10.1007/s10346-024-02298-6
- Wang, J., Xiao, L., Zhang, J., and Zhu, Y. (2019). Deformation characteristics and failure mechanisms of a rainfall-induced complex landslide in Wanzhou County, Three Gorges Reservoir, China. *Landslides* 17, 419–431. doi:10.1007/s10346-019-01317-1
- Yuan, Y., Xu, T., Heap, M. J., Meredith, P. G., Yang, T., and Zhou, G. (2021). A three-dimensional mesoscale model for progressive time-dependent deformation and fracturing of brittle rock with application to slope stability. *Computers and Geotechnics* 135, 104160. doi:10.1016/j.compgeo.2021.104160
- Zeng, F., Li, Y., and Labuz, J. (2018). Paul-Mohr-Coulomb failure criterion for geomaterials. *Journal of Geotechnical and Geoenvironmental Engineering* 144, 144. doi:10.1061/(asce)gt.1943-5606.0001829
- Zhang, L. M., Lü, Q., Deng, Z. H., and Wu, J. Y. (2024). Time-dependent probabilistic evaluation of rainstorm-induced shallow landslides considering influence of impermeable bedrock. *Georisk Assessment and Management of Risk for Engineered Systems and Geohazards* 19, 15–29. doi:10.1080/17499518.2024.2337383